Photoacoustics 40 (2024) 100653

Contents lists available at ScienceDirect

Photoacoustics

journal homepage: www.elsevier.com/locate/pacs

Machine learning radiomics based on intra and peri tumor PA/US images distinguish between luminal and non-luminal tumors in breast cancers

Sijie Mo [a,b,1], Hui Luo [a,b,1], Mengyun Wang [a,b], Guoqiu Li [a,b], Yao Kong [a,b], Hongtian Tian [a,b], Huaiyu Wu [a,b], Shuzhen Tang [a,b], Yinhao Pan [d], Youping Wang [e], Jinfeng Xu [a,b,*], Zhibin Huang [a,b,*], Fajin Dong [a,b,c,*]

[a] Department of Ultrasound, The Second Clinical Medical College, Jinan University, Guangdong 518020, China
[b] Department of Ultrasound, Shenzhen People's Hospital, Guangdong 518020, China
[c] Department of Ultrasound, The First Affiliated Hospital, Southern University of Science and Technology, Shenzhen, Guangdong 518020, China
[d] Mindray Bio-Medical Electronics Co.,Ltd., ShenZhen 518057,China
[e] Department of Clinical and Research, Shenzhen Mindray Bio-medical Electronics Co., Ltd., Shenzhen, China

ARTICLE INFO

Keywords:
Breast cancer
Molecular typing
Photoacoustic imaging
Radiomics
Ultrasound

ABSTRACT

Purpose: This study aimed to evaluate a radiomics model using Photoacoustic/ultrasound (PA/US) imaging at intra and peri-tumoral area to differentiate Luminal and non-Luminal breast cancer (BC) and to determine the optimal peritumoral area for accurate classification.

Materials and methods: From February 2022 to April 2024, this study continuously collected 322 patients at Shenzhen People's Hospital, using standardized conditions for PA/US imaging of BC. Regions of interest were delineated using ITK-SNAP, with peritumoral regions of 2 mm, 4 mm, and 6 mm automatically expanded using code from the Pyradiomic package. Feature extraction was subsequently performed using Pyradiomics. The study employed Z-score normalization, Spearman correlation for feature correlation, and LASSO regression for feature selection, validated through 10-fold cross-validation. The radiomics model integrated intra and peri-tumoral area, evaluated by receiver operating characteristic curve(ROC), Calibration and Decision Curve Analysis(DCA).

Results: We extracted and selected features from intratumoral and peritumoral PA/US images regions at 2 mm, 4 mm, and 6 mm. The comprehensive radiomics model, integrating these regions, demonstrated enhanced diagnostic performance, especially the 4 mm model which showed the highest area under the curve(AUC):0.898 (0.78–1.00) and comparably high accuracy (0.900) and sensitivity (0.937). This model outperformed the standalone clinical model and combined clinical-radiomics model in distinguishing between Luminal and non-Luminal BC, as evidenced in the test set results.

Conclusion: This study developed a radiomics model integrating intratumoral and peritumoral at 4 mm region PA/US model, enhancing the differentiation of Luminal from non-Luminal BC. It demonstrated the diagnostic utility of peritumoral characteristics, reducing the need for invasive biopsies and aiding chemotherapy planning, while emphasizing the importance of optimizing tumor surrounding size for improved model accuracy.

1. Introduction

Breast cancer (BC) is among the most common diseases affecting women worldwide and has been one of the diseases with the highest mortality rates in recent years [1,2]. As a disease characterized by its heterogeneity[3,4], BC has several recognized molecular subtypes, there

Abbreviations: BC, breast cancer; PA, Photoacoustic; US, ultrasound; IHC, immunohistochemistry ER: estrogen; PR, progesterone receptor; PA/US, Photoacoustic/ultrasound; CNB, core needle biopsy; MRI, magnetic resonance imaging; BI-RADS, Breast Imaging-Reporting and Data System; ROI, region of interest; STARD, Study of Diagnostic Accuracy Reporting; So2, oxygen saturation; LASSO, Least Absolute Shrinkage and Selection Operator; ROC, receiver operating characteristic curve; CI, confidence interval; AUC, area under the curve; DCA, Decision Curve Analysis; CDFI, Color Doppler Flow Imaging.

* Correspondence to: Department of Ultrasound, Shenzhen People's Hospital (The Second Clinical Medical College, Jinan University; The First Affiliated Hospital, Southern University of Science and Technology), Guangdong 518020, China.
E-mail addresses: xujinfeng@yahoo.com (J. Xu), zbhuangsz@gmail.com (Z. Huang), dongfajin@szhospital.com (F. Dong).
[1] These authors contributed equally to this work.

https://doi.org/10.1016/j.pacs.2024.100653
Received 14 July 2024; Received in revised form 6 September 2024; Accepted 20 September 2024
Available online 23 September 2024

are different treatment plans corresponding to these various molecular subtypes[5]. Luminal BC is more sensitive to hormone therapy and is less aggressive compared to non-Luminal types[6]. However, neoadjuvant chemotherapy may be more sensitive for non-luminal BC[7]. Researches have shown that neoadjuvant treatment plans, which are implemented after a pre-surgical diagnosis of BC, can improve survival rates for patients[5,7,8]. Consequently, the early detection of BC and the accurate identification of its molecular subtypes are essential for the personalized treatment and management of patients with BC.

Nowadays, type of BC is determined by immunohistochemistry (IHC) for estrogen (ER) and progesterone receptor (PR), human epidermal growth factor (Her2neu), and the proliferation marker Ki67[9,10], which are analyzed and categorized into these core indicators to obtain the accepted typology of BC: Luminal A, Luminal B, Her2-positive and triple-negative BC[11,12]. Null core needle biopsy (CNB) has been widely used in the diagnosis of BC, which can be used to determine the type of BC by IHC for biomarkers of BC before surgery. However, some researches have found that BC's heterogeneous nature can lead to discrepancies between the IHC results from preoperative biopsy and postoperative pathological specimens, especially on the bioindicator Her2 [13–15]. Such variations may impact the accurate molecular typing of BC potentially limiting the effectiveness of treatment options. Moreover, reanalyzing postoperative pathology samples of BC for IHC is not only costly but also a significant drain on medical resources[16].

Numerous non-invasive screening methods are available for detecting BC. Magnetic Resonance Imaging (MRI) is recognized for its heightened sensitivity in diagnosing BC, although it incurs higher costs and a significant false-positive rate[17]. Additionally, molybdenum target imaging excels in identifying BC calcifications but demonstrates a lower efficacy in detecting breast nodules[18]. Ultrasound (US) imaging, preferred by Asian populations for breast cancer screening, offers immediate, efficient, and radiation-free evaluations and allows for multi-angle assessments of breast nodules[19]. Despite these advantages, US imaging has limitations, such as the absence of functional lesions information and morphological overlaps that may lead to increased false positives[20,21]. Therefore, enhancing the accuracy of US screening in positively identifying breast cancer remains a significant challenge.

When combined with conventional US, photoacoustic (PA) imaging forms a synergistic diagnostic approach. In this method, PA emits laser light into the tissue, where it is primarily absorbed by hemoglobin, an intrinsic absorber, allowing for imaging[22,23]. This integration of PA and US technologies enables the capture of detailed morphological and functional information. Specifically, within the tumor environment of BC, which features neoplastic microvasculature, PA/US technology can quantitatively assess the oxygenation status of the tissues[24–26]. This capability addresses the limitation of conventional US, which alone lacks the ability to provide functional information about breast lesions. When diagnosing traditional breast cancer using grayscale ultrasound imaging, physicians often struggle to capture and utilize subtle image features visually. This limitation extends to photoacoustic images combined with grayscale ultrasound, where crucial photoacoustic signals may also be inadequately captured by the human eye. Therefore, there is an urgent need for developing an objective and accurate methodology to assess the clinical utility of PA imaging in the evaluation of breast lesions.

Radiomics is a method that extracts features quantitatively from images and constructs models using various machine learning algorithms. It enables the identification of features that are not readily recognizable or quantifiable by the naked eye, such as morphological features, texture, and intensity within image regions of interest (ROIs) [27]. Consequently, radiomics enhances the clinician's ability to make more informed decisions based on a detailed and quantifiable assessment of the image features. As an emerging technology, it has been applied to breast US images to preoperatively differentiate between Luminal-type and non-Luminal-type BC[23]. However, most studies have primarily focused on the intratumoral region, neglecting the peritumoral area. Given that breast cancer is an invasive tumor characterized by both intratumoral and peripheral stromal immune infiltrations, the peritumoral region could be crucial in distinguishing between Luminal and non-Luminal types of BC[28]. This region may contain significant diagnostic information absent in the intratumoral area alone. Despite its potential importance, few studies have analyzed the distinction between Luminal and non-Luminal types of BC based on combined intratumoral and peritumoral images from PA/US imaging.

Consequently, the primary objective of this study was to evaluate the diagnostic efficacy of a comprehensive breast-based intratumoral and peritumoral radiomics model of PA/US images for distinguishing between Luminal BC and non-Luminal BC. The secondary objective was to ascertain the optimal extent of the peritumoral area required for effective differentiation between Luminal BC and non-Luminal BC.

2. Materials and method

The study received approval from the ethics committee of the investigator's institution, under the ethical clearance number SYL-202161–02. Furthermore, all participants were fully informed about the study's objectives and procedures and provided their written informed consent. Adherence to the Standards for the Study of Diagnostic Accuracy Reporting (STARD) was maintained throughout the study to ensure the comprehensiveness, transparency, and reproducibility of the diagnostic findings[29]. These practices underscore our dedication to ethical research standards and the dependability of our results.

2.1. Study population

This study continuously collected data from 322 patients at Shenzhen People's Hospital, spanning from February 2022 to April 2024. The cohort was divided into two groups: 262 patients (mean age 50.42 ± 10.16 years) constituted the training set, and 60 patients (mean age 50.38 ± 9.33 years) formed the test set. All participants were enrolled under standardized conditions.

The exclusion criteria included: 1) absence of postoperative pathological data, 2) poor quality PA/US images, 3) presence of tumors other than BC, 4) patients with BC who had undergone radiotherapy or neoadjuvant chemotherapy within the past three months, 5) patients with psychiatric disorders impeding cooperation during clinical examinations, and 6) breast cancer patients presenting with open skin ulcers on their breasts. This study classified BC into Luminal and non-Luminal types, following the guidelines of the St. Gallen International Expert Consensus[30]. Fig. 1 is a flowchart of the patient inclusion process and Fig. 2 is a workflow diagram of the steps in the construction of the radiomics model.

2.2. PA/US imaging system and examination

The operators with at least ten years of experience in breast US conducted multimodal PA/US examinations using the Mindray L9–3 linear array probe outfitted with a custom-mounted divergent beam fiber. This configuration facilitated both the delivery of laser light and the detection of resulting photoacoustic signals. Photoacoustic imaging was performed using an OPO tunable laser (Spitlight 600-OPO, Innolas Laser GmbH)[31], which emits across a wavelength range of 680–980 nm. In this study, the wavelengths of 750 and 830 nm were utilized to quantify tissue oxygen saturation (So2), selected for their high absorption rates by deoxyhemoglobin and oxyhemoglobin, respectively (see Figure S1). This approach ensures enhanced precision in measuring the photoacoustic signals from the tissues. The detailed principles of the photoacoustic imaging system and corresponding procedural images are displayed in Appendix E1, Figures S2 and S3.

The environmental conditions during imaging were controlled, with the temperature set between 20 and 25℃ and humidity maintained at

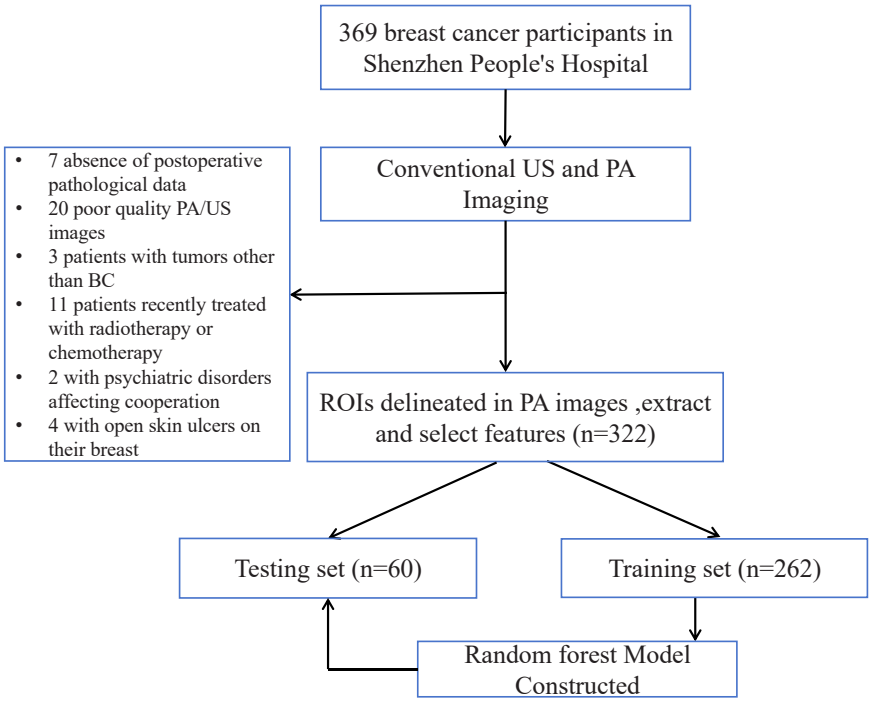

Fig. 1. Flowchart of patient inclusion and exclusion criteria.

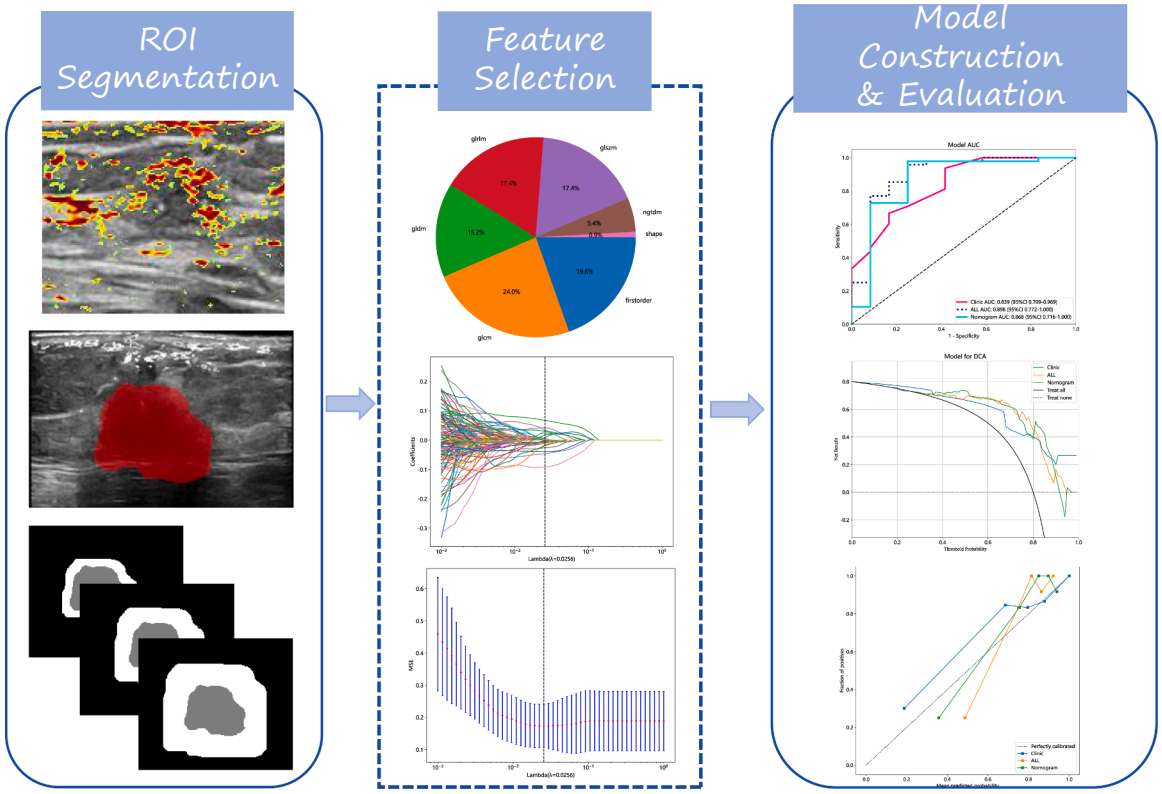

Fig. 2. ROI Segmentation. Note. Manual segmentation of the intratumoral area in PA/US images to define the ROI, followed by AI-assisted automatic segmentation of the peritumoral area at 2 mm, 4 mm, and 6 mm distances. Feature Selection: Features are extracted from the delineated PA/US images surrounding the tumor, with Lasso regression models employed for feature selection to optimize the analysis. Model Construction & Evaluation: Development of omics models based on the selected feature variables, which are then evaluated using AUC (Area Under the Curve) and DCA (Decision Curve Analysis) to assess the model's diagnostic performance.

50–70 % to ensure consistent imaging conditions. Patients were positioned supine with their arms abducted to 180° to fully expose the breast and axillary areas, optimizing probe access. The operator and participant wore protective eyewear for safety before the examination. Grayscale US is employed to identify breast lesions. To optimize acoustic coupling, an ultrasound gel pad is utilized. The probe is carefully aligned with the breast lesion to ensure clear imaging. Images are stabilized before being saved. This process includes capturing the largest cross-sectional area of the lesion and documenting its size and location for analysis. The detailed descriptions of the Standardization of Imaging Protocols and Quality Control of Examination during the process are displayed in Appendix E2.

2.3. ROI segmentation and feature extraction

All PA/US images of BC were included in the study, and ROIs within these images were delineated using ITK-SNAP software (version 3.8.0; [http://www.itksnap.org]). Two breast US operators, each with more than ten years of experience, independently outlined the PA/US images without knowledge of the pathological outcomes of the breast lesions. The intragroup correlation coefficient (ICC) was calculated using 60 randomly selected PA/US images to evaluate the reliability and reproducibility of the delineations. An ICC result greater than 0.75 indicates good agreement between the operators in delineating the ROIs region. For the peritumoral regions of 2 mm, 4 mm, and 6 mm, this study automated the expansion of the ROI using code from the Pyradiomic package. The delineated PA/US images were processed for feature extraction and selection, utilizing the Pyradiomics platform (https://pyradiomics.readthedocs.io/en/latest/index.html) to automatically extract radiomic features from each image. The normalization of the extracted features was performed using z-score normalization, and feature correlation was assessed using the Spearman correlation coefficient. Features with a correlation coefficient exceeding 0.9 were retained. Additionally, these features underwent the Mann-Whitney test, and any features with a p-value greater than 0.05 were eliminated. Feature selection continued through the Least Absolute Shrinkage and Selection Operator (LASSO) regression model applied to the training dataset. The LASSO method effectively reduces regression coefficients to zero, thereby assigning zero coefficients to many non-essential features based on the regularization parameter λ. The optimal λ was determined through a 10-fold cross-validation process using the minimum criteria method. Furthermore, the parameters of the retained non-zero coefficient features were incorporated into the regression model fitting.

2.4. Model construction and performance evaluation

Features selected via the LASSO regression model were utilized to construct intratumoral, peritumoral, and comprehensive radiomics models using the Random Forest machine learning algorithm, as is a highly efficient and widely used machine learning algorithm, to differentiate between Luminal and non-Luminal BC in the training set. The models were evaluated using metrics such as accuracy, sensitivity, and specificity to assess diagnostic efficacy. Additionally, a clinical prediction model was developed to predict Luminal and non-Luminal type BC in the training set, incorporating clinical variables such as intratumoral So2, lesion location, BI-RADS classification, peritumoral and intratumoral CDFI, boundary, Echo pattern, and lymph node metastasis. Ultimately, an integrated model combining both radiomics and clinical data was constructed. The diagnostic performance of each model was assessed using ROC curves, the clinical utility was determined through Decision Curve Analysis (DCA) and calibration curve.

2.5. Statistical analysis

Statistical analysis was performed using R 4.2.2(Copyright (C) 2022 The R Foundation for Statistical Computing). The utilizing a two-sided p-value threshold of less than 0.05 to determine statistical significance. Continuous variables were presented as mean ± standard deviation for descriptive statistics, while categorical variables were expressed as median (interquartile range) and frequency (%). The Mann-Whitney U test was used for continuous variables, and depending on the stratification of the dataset, categorical variables were analyzed using either the chi-squared test or Fisher's exact test.

3. Results

3.1. Clinical results

This study included a total of 322 patients, with 262 in the training set and 60 in the test set. Postoperative pathology identified 247 cases of Luminal BC and 75 cases of non-Luminal BC. Clinical variables are presented in Table 1. Variables such as Year, Height, Weight, BMI, menopause status, Location, BI-RADS category, Lymph Node Metastasis, Lesion Maximum Diameter, External Color Doppler Flow Imaging (External CDFI), Internal Color Doppler Flow Imaging (Internal CDFI), Boundary, and Posterior features showed no statistically significant differences between the training and test sets($P>0.05$). Characteristic selection of clinical variables was performed and significant variables were identified by univariate regression analysis (see Table 2). The Univariable analysis screened for External CDFI($P<0.01$), Internal CDFI ($P<0.01$), Echo pattern ($P<0.01$), Lymph Node Metastasis($P=0.024$) as variables with higher correlation. These variables were then further analyzed using multivariate regression analysis to identify variables with high correlation in distinguishing between Luminal BC and non-Luminal BC, and finally a clinical model was constructed that was characterized by Internal CDFI($P=0.02$), Echo pattern ($P=0.015$), Lymph Node Metastasis($P=0.016$) as the main clinical variable. The diagnostic efficacy of the clinical model with test set and training set is demonstrated in Table 3 and Appendix Table 1, where we found that in the training set, the area under the curve (AUC) value of the model was 0.868 (0.82–0.91) and the accuracy, sensitivity and specificity were 0.653, 0.568 and 0.921, respectively, and it is noteworthy that the AUC (95 % Cl) of its test set was 0.839 (0.71–0.97) and sensitivity (0.812) is higher than the training set. The accuracy and specificity of the clinical model test set were 0.767 and 0.583, respectively. And the ROC curve of clinical model is shown in Figure S4.

3.2. Intratumoral peritumoral radiomics model's construction and results

Based on PA/US images from intratumoral and peritumoral regions at 2 mm, 4 mm, and 6 mm, we extracted 1561 features across these images and subsequently performed feature selection from each group. Through LASSO dimensionality reduction, 30 features were selected from the intratumoral region, and 30, 27, and 23 features from the peritumoral regions at 2 mm, 4 mm, and 6 mm, respectively. We constructed composite radiomics models integrating intratumoral with peritumoral 2 mm, 4 mm, and 6 mm regions to quantitatively assess the differences between Luminal and non-Luminal BC. The results of these models in the test set and training set are presented in Table 3 and Appendix Table 1. The intratumoral model exhibited an AUC (95 % CI) of 0.712 (0.51–0.91) in test set, with a sensitivity of 0.937 and specificity of 0.500, indicating limited diagnostic effectiveness. The ROC curve of intratumoral model is shown on Figure S5. Conversely, the intratumoral model combining with peritumoral regions at 2 mm, 4 mm, and 6 mm demonstrated enhanced diagnostic performance. The ROC curves for each model are shown in Figure S6, Fig. 3, and Figure S7, respectively. Specifically, the 2 mm model achieved an AUC (95 % CI) of 0.690 (0.49–0.89) in the test set, with sensitivity and specificity of 0.542 and 0.833, respectively. The 4 mm model recorded an AUC (95 % CI) of 0.898 (0.78–1.00), with sensitivity and specificity of 0.937 and 0.750, respectively. In the test set, the 6 mm model reached an AUC (95 % CI) of 0.766(0.57–0.96), with sensitivity and specificity of 0.937 and 0.667,

Table 1
Baseline Characteristics of the Training and Test Sets.

Variables	Total (n = 322)	Training Set (n = 262)	Test Set (n = 60)	P value
Molecular type, n (%)				0.617
Luminal	247 (77)	199 (76)	48 (80)	
Non-Luminal	75 (23)	63 (24)	12 (20)	
Year	50 (44, 57)	50 (44, 57)	49 (43, 57.25)	0.507
Height	160 (155, 163)	160 (155, 163)	160 (155, 163)	0.443
Weigh	60 (52, 63)	60 (52, 64)	56.5 (52, 62)	0.116
BMI	23.33 (20.33, 25)	23.43 (20.4, 25)	22.67 (20.3, 24.2)	0.183
Menstruation, n (%)				0.604
No	166 (52)	133 (51)	33 (56)	
Yes	153 (48)	127 (49)	26 (44)	
Location, n (%)				0.960
Left	170 (53)	139 (53)	31 (52)	
Right	152 (47)	123 (47)	29 (48)	
BI-RADS, n (%)				0.688
4a	52 (16)	41 (16)	11 (18)	
4b	66 (20)	51 (19)	15 (25)	
4c	169 (52)	141 (54)	28 (47)	
5	35 (11)	29 (11)	6 (10)	
Lymph Node Metastasis, n (%)				0.788
No	218 (68)	176 (67)	42 (70)	
Yes	104 (32)	86 (33)	18 (30)	
Max	19 (14, 26)	19.5 (14, 26)	19 (15, 23)	1.000
External CDFI, n (%)				0.841
No detectable blood	19 (6)	16 (6)	3 (5)	
Hypo vascular Blood	132 (41)	104 (40)	28 (47)	
Hyper vascular Blood	77 (24)	64 (24)	13 (22)	
Rich Blood	94 (29)	78 (30)	16 (27)	
Internal CDFI, n (%)				0.501
No detectable blood	48 (15)	36 (14)	12 (20)	
Hypo vascular Blood	116 (36)	93 (35)	23 (38)	
Hyper vascular Blood	69 (21)	59 (23)	10 (17)	
Rich Blood	89 (28)	74 (28)	15 (25)	
Boundary, n (%)				1.000
Not clear	62 (19)	50 (19)	12 (20)	
Clear	260 (81)	212 (81)	48 (80)	
Echo pattern, n (%)				0.379
Ultra-hypoechoic	139 (43)	113 (43)	26 (43)	
Hypoechoic	178 (55)	146 (56)	32 (53)	
Complex cystic and solid Hyperechoic	5 (2)	3 (1)	2 (3)	
Posterior features, n (%)				0.445
Shadowing	97 (30)	83 (32)	14 (23)	
No posterior features	151 (47)	120 (46)	31 (52)	
Enhancement	74 (23)	59 (23)	15 (25)	

Note. BI-RADS: Breast Imaging-Reporting and Data System; External CDFI: External Color Doppler Flow Imaging; Internal CDFI: Internal Color Doppler Flow Imaging.

Table 2
Univariable and Multivariable analyses of the clinical characteristics and clinicopathologic features in patients in the training set.

variables	OR (95 %CI)	P value	OR (95 %CI)	P value
	Univariate		Multivariate	
Echo Pattern	0.837(0.77,0.908)	<0.010	0.884 (0.812,0.961)	0.015
Lymph Node Metastasis	0.881(0.803,0.967)	0.024	0.878 (0.804,0.959)	0.016
Boundary	0.905(0.811,1.011)	0.140		
BI-RADS	0.966(0.919,1.015)	0.251		
So2	1(0.999,1.001)	0.484		
Location	1.024(0.939,1.119)	0.649		
External CDFI	1.123(1.074,1.175)	<0.010	0.981 (0.893,1.078)	0.740
Internal CDFI	1.138(1.093,1.185)	<0.010	1.132 (1.038,1.236)	0.020

Note. So2: oxygen saturation; External CDFI: External Color Doppler Flow Imaging; BI-RADS: Breast Imaging-Reporting and Data System; Internal CDFI: Internal Color Doppler Flow Imaging; CI: confidence interval; OR: Odds Ratio.

Table 3
Diagnostic performance of radiomics models in test set.

Model	AUC (95 % CI)	Accuracy	Sensitivity	Specificity
Clinical	0.839 (0.71–0.97)	0.767	0.812	0.583
Intra	0.712 (0.51–0.91)	0.850	0.937	0.500
2 mm (Intra+Peri)	0.690 (0.49–0.89)	0.600	0.542	0.833
4 mm (Intra+Peri)	0.898 (0.78–1.00)	0.900	0.937	0.750
6 mm (Intra+Peri)	0.766 (0.57–0.96)	0.883	0.937	0.667
Clinical+Intra+4mmPeri	0.868 (0.72 – 1.00)	0.917	0.985	0.750

Note. AUC: area under the curve; CI: confidence interval; Intra: Intratumoral; Peri: Peritumoral.

The Figure Legends

respectively. Among these models, the model of 4 mm peritumoral region combining intratumoral model demonstrated the highest diagnostic performance.

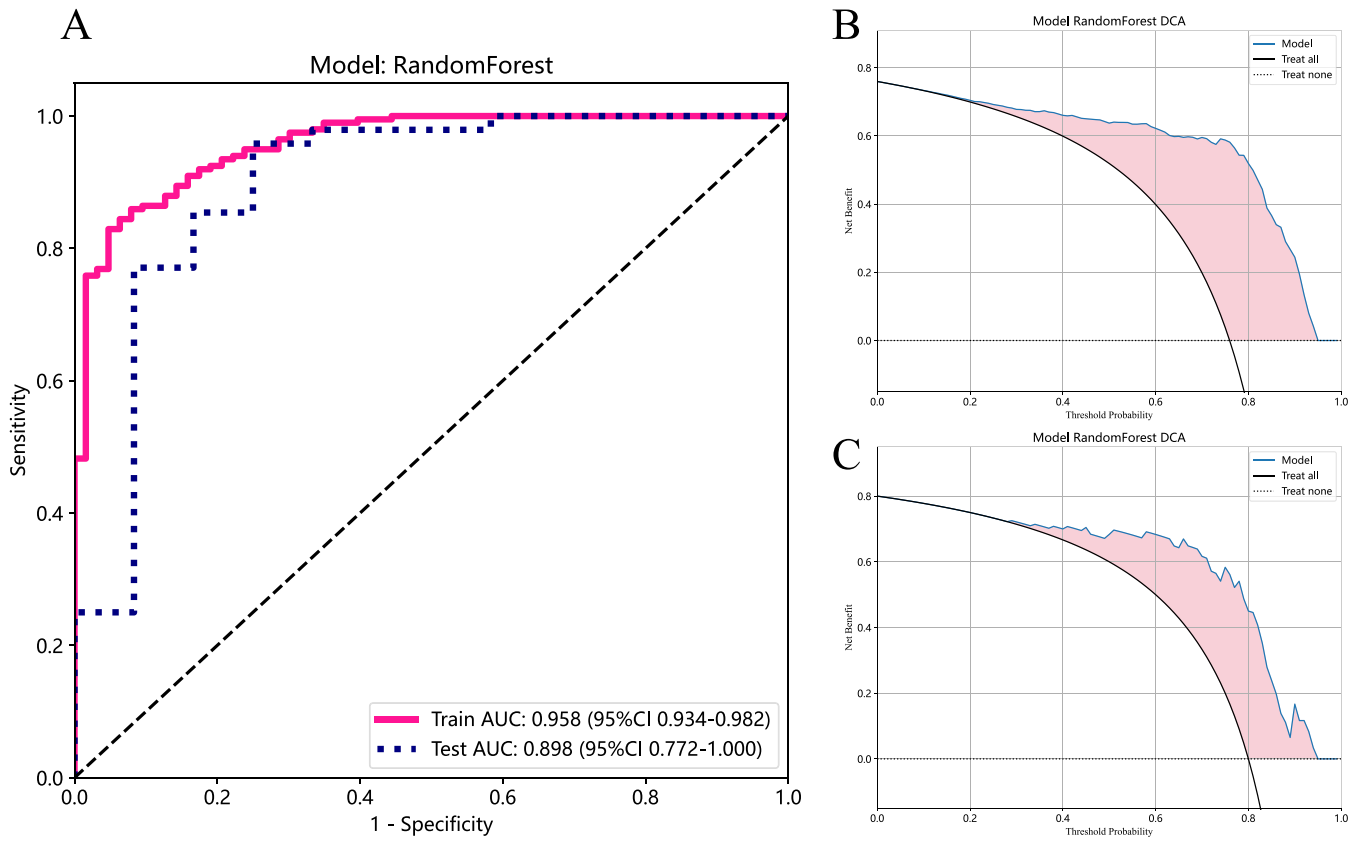

Fig. 3. Evaluation of diagnostic performance of intratumor combined with 4 mm peritumoral area. Note. Fig. A displays the ROC curve for the fusion model combining the intratumoral model with the 4 mm peritumoral region. Figs. B and C depict the DCA for the training and testing sets of the model, respectively.

3.3. Results of integrating radiomics and clinical models

Therefore, combining the intra-peritumoral at 4 mm regions model and clinical model, we constructed the comprehensive model, which shown as nomogram model (see Figs. 4A and 4B). This nomogram model achieved an AUC (95 % CI) of 0.868 (0.72 – 1.00) in the test set, with an accuracy of 0.917, sensitivity of 0.958, and specificity of 0.750. Although the AUC of this model is not the highest, it has the highest accuracy and sensitivity. And its specificity is comparable to other models. However, compared to the standalone clinical model and the combined clinical and intra-peritumoral model at 4 mm, the intratumoral and 4 mm peritumoral model demonstrates superior diagnostic performance for distinguishing between Luminal and non-Luminal BC. The performance of the DCA for the various models in training and test sets is illustrated in Figs. 4C and 4D. It was observed that the intra-peritumoral mode exhibits enhanced clinical value in both the training and test sets. The calibration curves for the various models are depicted in Figs. 4E and 4F, quantifying the congruence between the model's predicted probabilities and the actual observed outcomes. Notably, the calibration curve of the clinical model in test set closely approximates the ideal curve, indicating superior predictive accuracy.

4. Discussion

Multimodal PA/US imaging has been recognized for its utility in diagnosing breast tumors[25,32–34]. Dogan et al. [35] highlighted the correlation between photoacoustic imaging features and the molecular classification of breast cancer, particularly distinguishing between invasive and noninvasive types. While previous studies primarily relied on subjective, naked-eye scoring of PA image features and grayscale US image features to explore correlations with BC molecular types, comprehensive and objective analysis using PA/US images has been less frequently addressed[36]. In our study, we employed quantitative feature extraction and analysis from tumor PA/US images across intratumoral and various peritumoral regions (2 mm, 4 mm, and 6 mm) to more thoroughly and objectively assess the association of photoacoustic imaging with Luminal BC and non-Luminal BC, which includes triple-negative breast cancer and HER2 overexpression. We developed a comprehensive Nomogram model that integrates clinical features with radiomics features. Notably, the model for the intratumoral and 4 mm peritumoral region exhibited superior diagnostic efficacy, achieving an AUC (95 % CI) of 0.898 (0.78–1.00) in the test set. This performance surpassed that of the single clinical model, which recorded an AUC (95 % CI) of 0.839 (0.71–0.97), and the nomogram model in the test set, which achieved an AUC (95 % CI) of 0.868 (0.72 – 1.00).

Previous studies on radiomics in BC molecular typing have focused on deriving information and features from the intratumoral region to differentiate between Luminal BC and non-Luminal BC[37,38]. However, with advances in biomedical science, increasing evidence has highlighted the significant correlation between the tumor microenvironment and cancer cell behaviors such as unchecked proliferation and evasion of immune mechanisms, suggesting that the peritumoral regions can also provide valuable information[39]. In addition, the results of this study shown that, the AUC (95 % CI) of the model based solely on intratumoral features was only 0.712 (0.51–0.91) in the test set, whereas the models that combined intratumoral with peritumoral features consistently achieved AUC values above 0.8, showing a clear improvement. This further demonstrates that the peritumoral region of breast tumors contains valuable information for distinguishing between Luminal and non-Luminal BC. The research by SX Niu and others, which evaluated molecular typing radiomics based on breast X-ray and MRI images, constructed a model incorporating intratumoral and peritumoral assessments[40]. This model demonstrated AUCs ranging from 0.6 to 0.8 for predicting the four molecular subtypes of BC in the test set,

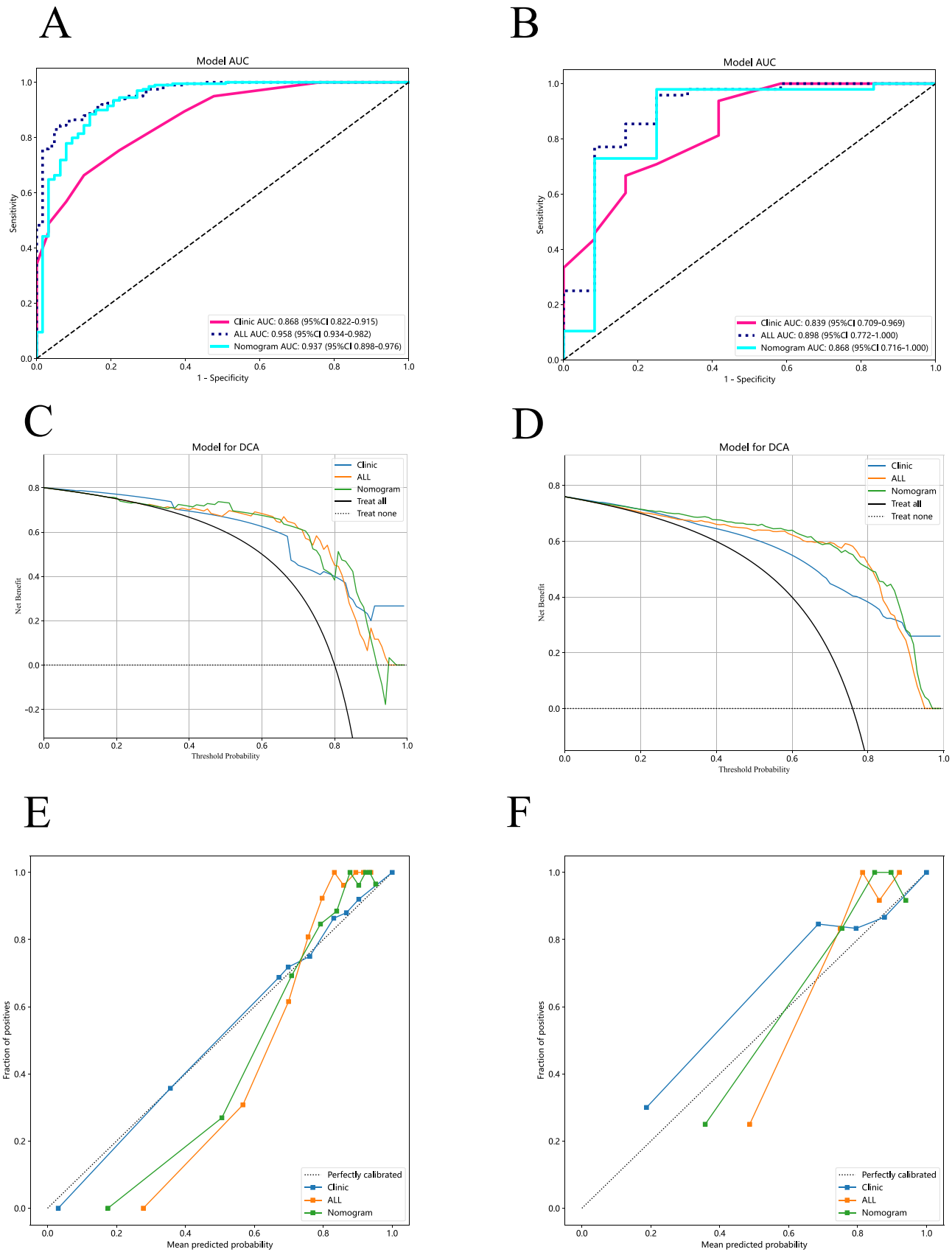

Fig. 4. Evaluation of diagnostic performance of the comprehensive model. Note. Clinic: clinical model; All: intratumoral + peritumoral radiomics model; Nomogram: clinical model + All (intratumoral + peritumoral radiomics model); Figs. A and B display the ROC curves for the clinical models, intratumoral and 4 mm peritumoral fusion models, and their combined models, where A represents the AUC for the training set and B represents the AUC for the testing set. Figs. C and D illustrate the DCA for the training and testing sets of each model, respectively, while Figs E and F depict the calibration curves for the training and testing sets of each model, respectively.

similar to the intratumoral and 4 mm peritumoral model's AUC (95 % CI) of 0.898 (0.78–1.00) in this study. However, breast MRI is expensive and not the preferred option for breast cancer screening, and the X-ray imaging carries inherent risks, thus, their clinical utility in predicting Luminal and non-Luminal BC is relatively limited. In contrast, a significant advantage of using PA/US imaging in this study is its harmlessness to patients, along with its convenience and accessibility. Moreover, research focusing on the diagnostic efficacy of radiomics through ultrasound imaging for intratumoral and peritumoral areas of breast tumors remains limited. Additionally, no studies have yet concentrated on combining radiomic models of intratumoral and peritumoral regions with clinical models to differentiate between Luminal BC and non-Luminal BC. Therefore, this study integrated the intratumoral and surrounding peritumoral areas of BC, constructed a comprehensive radiomic and clinical model using machine learning algorithms, and compared the diagnostic efficacy of different models for Luminal BC and non-Luminal BC.

Given the emerging nature of PA imaging, there is significant potential to advance its application in the molecular typing of BC using PA/US. L. Lin et al. observed through the SBH PACT system that vascular density is higher in breast tumor tissues compared to normal tissues, and that the vascular architecture in tumors is disorganized and unevenly distributed[41]. These findings align with the objectives of this study, which utilizes PA/US images to develop a radiomic model for the quantitative analysis of BC molecular types. This model demonstrated a high AUC value in the test set, indicating good diagnostic efficiency for distinguishing between Luminal and non-Luminal BC. The effectiveness of the model may stem from its ability to identify distinct vascular patterns and densities associated with varying invasion levels of Luminal and non-Luminal BC (HER2 positive and triple-negative BC), which can be effectively captured by radiomic models.

Furthermore, this study discovered that among the clinical model, intratumoral and peritumoral radiomics model, and the nomogram model, all three demonstrated a high capacity to differentiate between Luminal BC and non-Luminal BC. Interestingly, it was not the nomogram model, which integrates clinical and radiomics data, that showed the highest diagnostic performance in the test set with an AUC (95 % CI) of 0.868 (0.72–1.00), but rather the intratumoral and peritumoral radiomics model, which achieved the best diagnostic efficacy with an AUC (95 % CI) of 0.898 (0.78–1.00). This intriguing outcome aligns with similar findings from other studies, and conclusions from this multicenter study indicate that the addition of radiomics models did not enhance the diagnostic efficacy of clinical models[42]. Therefore, in this study, ensuring the robustness of each model and without overfitting, the high diagnostic efficiency of the radiomics model is reasonable. This is one of the innovative points of this research.

What's more, we focused on peritumoral regions of 2 mm, 4 mm, and 6 mm for feature extraction in this study. The 4 mm region was deemed optimal as the 2 mm region often lacks sufficient data to adequately reflect BC aggressiveness and the nuances conveyed by photoacoustic signals, while the 6 mm region may incorporate excessive normal breast tissue, potentially diluting diagnostic precision for distinguishing between Luminal and Non-Luminal BC types. Furthermore, the central frequency of our imaging probe was set at 5.5 MHz. Research has shown that the probe's frequency can significantly affect the performance of AI diagnostic models, as it influences the quality of the extracted image features essential for robust radiomic analysis[43]. However, our study was limited to a single probe type, which restricts a thorough exploration of frequency effects on image quality and diagnostic utility. In conclusion, the results of this study not only reinforce the utility of peritumoral features in radiomics based on PA imaging but also highlight that the selection of peritumoral region size significantly influences the predictive outcomes of radiomics analysis.

This study is subject to several limitations. First, it is a single-center study, which may introduce bias. Expanding the sample size or incorporating data from other centers for external validation could enhance the diagnostic performance of the model and mitigate bias. Second, the delineation of ROI regions in PA/US images is not fully automated. Although dual-person delineation was employed to ensure consistency, potential biases could still be present. Implementing AI for automatic delineation of ROI regions could address this issue. Additionally, this study did not incorporate a grayscale US-based radiomics model of the area surrounding the BC tumor for comparison. In future research, including this model could improve the comprehensiveness and rigor of the study. Finally, as a continuous collected study, changes in practice, diagnostic criteria, and techniques over time may influence the correlation and applicability of the research findings. Future research should involve a well-designed experimental plan and prospective data collection to verify the feasibility of the study's approach.

5. Conclusion

This study developed a radiomics model utilizing intratumoral and peritumoral features derived from PA/US images of BC, facilitating the analysis and differentiation of Luminal BC from non-Luminal BC. It confirmed that the peritumoral region harbors characteristic information pertinent to the molecular typing of BC. Moreover, the intra-peritumoral radiomics model established in this study offers an auxiliary diagnostic method that aids in the formulation of neoadjuvant chemotherapy regimens and reduces the necessity for invasive biopsy procedures in patients with BC. And our study highlights the critical impact of the selection of tumor surrounding size on the predictive accuracy of radiomics models. In particular, the radiomics model of intratumoral and the 4 mm peritumoral area demonstrated the highest diagnostic efficacy for distinguishing between Luminal and non-Luminal BC. It underscores the necessity to optimize tumor surrounding features in future radiomics research, with the aim of enhancing the overall predictive performance of these models.

Financial support

No.

CRediT authorship contribution statement

Guoqiu Li: Methodology, Investigation, Conceptualization. **Fajin Dong:** Supervision, Resources, Investigation, Data curation. **Sijie Mo:** Writing – original draft, Methodology, Formal analysis, Data curation. **Youping Wang:** Investigation, Methodology. **Mengyun Wang:** Resources, Methodology, Formal analysis, Data curation. **Huaiyu Wu:** Visualization, Resources, Project administration. **Hui Luo:** Resources, Data curation, Formal analysis. **Yao Kong:** Resources, Investigation, Data curation. **Hongtian Tian:** Validation, Supervision, Investigation. **Jinfeng Xu:** Supervision, Resources. **Zhibin Huang:** Software, Resources, Methodology, Investigation. **Yinhao Pan:** Methodology, Formal analysis. **Shuzhen Tang:** Resources.

Declaration of Competing Interest

The authors declare that they have no known competing financial interests or personal relationships that could have appeared to influence the work reported in this paper.

Data Availability

Data will be made available on request.

Acknowledgments

This project was supported by Shenzhen Science and Technology Program(GJHZ20240218114504009).

Main author's contribution

Sijie Mo, the first author and Hui Luo, the co-first authors, also contributed to this work by conceiving and designing the experiments, analyzing the data, and providing materials/analytical tools. Jinfeng Xu, Zhibin Huang and Fajin Dong are the corresponding authors and the guarantors of the integrity of the entire study. All authors approved the final version to be published.

Appendix A. Supporting information

Supplementary data associated with this article can be found in the online version at doi:10.1016/j.pacs.2024.100653.

References

[1] N. Jokhadze, A. Das, D.S. Dizon, Global cancer statistics: a healthy population relies on population health, CA Cancer J. Clin. (2024).
[2] R.L. Siegel, A.N. Giaquinto, A. Jemal, Cancer statistics, 2024, CA Cancer J. Clin. 74 (1) (2024) 12–49.
[3] A. Roulot, D. Héquet, J.-M. Guinebretière, A. Vincent-Salomon, F. Lerebours, C. Dubot, R. Rouzier, Tumoral heterogeneity of breast cancer, Ann. Biol. Clin. (Paris 74 (6) (2016) 653–660.
[4] Y. Liang, H. Zhang, X. Song, Q. Yang, Metastatic heterogeneity of breast cancer: molecular mechanism and potential therapeutic targets, Semin Cancer Biol. 60 (2020) 14–27.
[5] Effects of chemotherapy and hormonal therapy for early breast cancer on recurrence and 15-year survival: an overview of the randomised trials, Lancet 365 (9472) (2005) 1687–1717.
[6] P.H. Cottu, [Systemic neoadjuvant therapy of luminal breast cancer in 2016], Bull. Cancer 104 (1) (2017) 69–78.
[7] M. Sirico, A. Virga, B. Conte, M. Urbini, P. Ulivi, C. Gianni, F. Merloni, M. Palleschi, M. Gasperoni, A. Curcio, et al., Neoadjuvant endocrine therapy for luminal breast tumors: state of the art, challenges and future perspectives, Crit. Rev. Oncol. Hematol. 181 (2023) 103900.
[8] M.K. Barton, Bevacizumab in neoadjuvant chemotherapy increases the pathological complete response rate in patients with triple-negative breast cancer, CA Cancer J. Clin. 64 (3) (2014) 155–156.
[9] T. Bonacho, F. Rodrigues, J. Liberal, Immunohistochemistry for diagnosis and prognosis of breast cancer: a review, Biotech. Histochem 95 (2) (2020) 71–91.
[10] A.C. Wolff, M.E.H. Hammond, K.H. Allison, B.E. Harvey, P.B. Mangu, J.M. S. Bartlett, M. Bilous, I.O. Ellis, P. Fitzgibbons, W. Hanna, et al., Human Epidermal Growth Factor Receptor 2 Testing in Breast Cancer: American Society of Clinical Oncology/College of American Pathologists Clinical Practice Guideline Focused Update, J. Clin. Oncol. 36 (20) (2018) 2105–2122.
[11] P. Das, G.M. Siegers, L.-M. Postovit, Illuminating luminal B: QSOX1 as a subtype-specific biomarker, Breast Cancer Res 15 (3) (2013) 104.
[12] A. Goldhirsch, E.P. Winer, A.S. Coates, R.D. Gelber, M. Piccart-Gebhart, B. Thürlimann, H.J. Senn, Personalizing the treatment of women with early breast cancer: highlights of the St Gallen International Expert Consensus on the Primary Therapy of Early Breast Cancer 2013, Ann. Oncol. 24 (9) (2013) 2206–2223.
[13] M. Pölcher, M. Braun, M. Tischitz, M. Hamann, N. Szeterlak, A. Kriegmair, C. Brambs, C. Becker, O. Stoetzer, Concordance of the molecular subtype classification between core needle biopsy and surgical specimen in primary breast cancer, Arch. Gynecol. Obstet. 304 (3) (2021) 783–790.
[14] I. Meattini, G. Bicchierai, C. Saieva, D. De Benedetto, I. Desideri, C. Becherini, D. Abdulcadir, E. Vanzi, C. Boeri, S. Gabbrielli, et al., Impact of molecular subtypes classification concordance between preoperative core needle biopsy and surgical specimen on early breast cancer management: single-institution experience and review of published literature, Eur. J. Surg. Oncol.: J. Eur. Soc. Surg. Oncol. Br. Assoc. Surg. Oncol. 43 (4) (2017) 642–648.
[15] X. Chen, L. Sun, Y. Mao, S. Zhu, J. Wu, O. Huang, Y. Li, W. Chen, J. Wang, Y. Yuan, et al., Preoperative core needle biopsy is accurate in determining molecular subtypes in invasive breast cancer, BMC Cancer 13 (2013) 390.
[16] N. Naik, A. Madani, A. Esteva, N.S. Keskar, M.F. Press, D. Ruderman, D.B. Agus, R. Socher, Deep learning-enabled breast cancer hormonal receptor status determination from base-level H&E stains, Nat. Commun. 11 (1) (2020) 5727.
[17] C.K. Kuhl, A. Keulers, K. Strobel, H. Schneider, N. Gaisa, S. Schrading, Not all false positive diagnoses are equal: on the prognostic implications of false-positive diagnoses made in breast MRI versus in mammography / digital tomosynthesis screening, Breast Cancer Res 20 (1) (2018) 13.
[18] D. Wekking, M. Porcu, P. De Silva, L. Saba, M. Scartozzi, C. Solinas, Breast MRI: clinical indications, recommendations, and future applications in breast cancer diagnosis, Curr. Oncol. Rep. 25 (4) (2023) 257–267.
[19] R. Guo, G. Lu, B. Qin, B. Fei, Ultrasound imaging technologies for breast cancer detection and management: a review, Ultrasound Med Biol. 44 (1) (2018) 37–70.
[20] N. Ohuchi, A. Suzuki, T. Sobue, M. Kawai, S. Yamamoto, Y.-F. Zheng, Y.N. Shiono, H. Saito, S. Kuriyama, E. Tohno, et al., Sensitivity and specificity of mammography and adjunctive ultrasonography to screen for breast cancer in the Japan Strategic Anti-cancer Randomized Trial (J-START): a randomised controlled trial, Lancet 387 (10016) (2016) 341–348.
[21] A.S. Tagliafico, M. Calabrese, G. Mariscotti, M. Durando, S. Tosto, F. Monetti, S. Airaldi, B. Bignotti, J. Nori, A. Bagni, et al., Adjunct screening with tomosynthesis or ultrasound in women with mammography-negative dense breasts: interim report of a prospective comparative trial, J. Clin. Oncol. 34 (16) (2016) 1882–1888.
[22] K.S. Valluru, K.E. Wilson, J.K. Willmann, Photoacoustic Imaging in Oncology: Translational Preclinical and Early Clinical Experience, Radiology 280 (2) (2016) 332–349.
[23] B.E. Dogan, G.L.G. Menezes, R.S. Butler, E.I. Neuschler, R. Aitchison, P.T. Lavin, F. L. Tucker, S.R. Grobmyer, P.M. Otto, A.T. Stavros, Optoacoustic imaging and gray-scale US features of breast cancers: correlation with molecular subtypes, Radiology 292 (3) (2019) 564–572.
[24] K. Lundgren, C. Holm, G. Landberg, Hypoxia and breast cancer: prognostic and therapeutic implications, Cell Mol. Life Sci. 64 (24) (2007) 3233–3247.
[25] N. Nyayapathi, J. Xia, Photoacoustic imaging of breast cancer: a mini review of system design and image features, J. Biomed. Opt. 24 (12) (2019).
[26] Z. Huang, H. Tian, H. Luo, K. Yang, J. Chen, G. Li, Z. Ding, Y. Luo, S. Tang, J. Xu, et al., Assessment of oxygen saturation in breast lesions using photoacoustic imaging: correlation with benign and malignant disease, Clin. Breast Cancer (2024).
[27] A. Conti, A. Duggento, I. Indovina, M. Guerrisi, N. Toschi, Radiomics in breast cancer classification and prediction, Semin Cancer Biol. 72 (2021) 238–250.
[28] M.V. Dieci, F. Miglietta, V. Guarneri, Immune infiltrates in breast cancer: recent updates and clinical implications, Cells 10 (2) (2021).
[29] Bossuyt, P.M. Reitsma, J.B. Bruns DE, C.A. Gatsonis, P.P. Glasziou, L. Irwig, J. G. Lijmer, D. Moher, D. Rennie, H.C.W. de Vet, et al., STARD 2015: an updated list of essential items for reporting diagnostic accuracy studies, Clin. Chem. 61 (12) (2015) 1446–1452.
[30] A. Goldhirsch, W.C. Wood, A.S. Coates, R.D. Gelber, B. Thürlimann, H.J. Senn, Strategies for subtypes–dealing with the diversity of breast cancer: highlights of the St. Gallen International Expert Consensus on the Primary Therapy of Early Breast Cancer 2011. Ann. Oncol. 22 (8) (2011) 1736–1747.
[31] M. Wang, L. Zhao, Y. Wei, J. Li, Z. Qi, N. Su, C. Zhao, R. Zhang, T. Tang, S. Liu, et al., Functional photoacoustic/ultrasound imaging for the assessment of breast intraductal lesions: preliminary clinical findings, Biomed. Opt. Express 12 (3) (2021) 1236–1246.
[32] K. Kratkiewicz, A. Pattyn, N. Alijabbari, M. Mehrmohammadi, Ultrasound and photoacoustic imaging of breast cancer: clinical systems, challenges, and future outlook, J. Clin. Med 11 (5) (2022).
[33] S. Manohar, M. Dantuma, Current and future trends in photoacoustic breast imaging, Photoacoustics 16 (2019) 100134.
[34] Z. Huang, S. Mo, H. Wu, Y. Kong, H. Luo, G. Li, J. Zheng, H. Tian, S. Tang, Z. Chen, et al., Optimizing breast cancer diagnosis with photoacoustic imaging: an analysis of intratumoral and peritumoral radiomics, Photoacoustics 38 (2024) 100606.
[35] R. Li, Peritumoral radiomics and predicting treatment response, JAMA Netw. Open 3 (9) (2020) e2016125.
[36] R.M. Mann, Do we need optoacoustic assessment of hypoxia to differentiate molecular subtypes of breast cancer? Radiology 292 (3) (2019) 573–574.
[37] S. Feng, J. Yin, Dynamic contrast-enhanced magnetic resonance imaging radiomics analysis based on intratumoral subregions for predicting luminal and nonluminal breast cancer, Quant. Imaging Med Surg. 13 (10) (2023) 6735–6749.
[38] Y. Huang, Z. Yao, L. Li, R. Mao, W. Huang, Z. Hu, Y. Hu, Y. Wang, R. Guo, X. Tang, et al., Deep learning radiopathomics based on preoperative US images and biopsy whole slide images can distinguish between luminal and non-luminal tumors in early-stage breast cancers, EBioMedicine 94 (2023) 104706.
[39] N. Braman, P. Prasanna, J. Whitney, S. Singh, N. Beig, M. Etesami, D.D.B. Bates, K. Gallagher, B.N. Bloch, M. Vulchi, et al., Association of peritumoral radiomics with tumor biology and pathologic response to preoperative targeted therapy for HER2 (ERBB2)-positive breast cancer, JAMA Netw. Open 2 (4) (2019) e192561.
[40] S. Niu, W. Jiang, N. Zhao, T. Jiang, Y. Dong, Y. Luo, T. Yu, X. Jiang, Intra- and peritumoral radiomics on assessment of breast cancer molecular subtypes based on mammography and MRI, J. Cancer Res Clin. Oncol. 148 (1) (2022).
[41] L. Lin, X. Tong, P. Hu, M. Invernizzi, L. Lai, L.V. Wang, Photoacoustic computed tomography of breast cancer in response to neoadjuvant chemotherapy, Adv. Sci. (Weinh.) 8 (7) (2021) 2003396.
[42] F. Moro, M. Albanese, L. Boldrini, V. Chiappa, J. Lenkowicz, F. Bertolina, F. Mascilini, R. Moroni, M.A. Gambacorta, F. Raspagliesi, et al., Developing and validating ultrasound-based radiomics models for predicting high-risk endometrial cancer, Ultrasound Obstet. Gynecol. 60 (2) (2022) 256–268.
[43] Z. Huang, K. Yang, H. Tian, H. Wu, S. Tang, C. Cui, S. Shi, Y. Jiang, J. Chen, J. Xu, et al., A validation of an entropy-based artificial intelligence for ultrasound data in breast tumors, BMC Med Inf. Decis. Mak. 24 (1) (2024) 1.

Xu Jinfeng, MD, Chief Physician, Professor of Second Clinical Medical College, Jinan University, Supervisor of Master's, Doctoral, and Postdoctoral candidates. Member of the Ultrasound Medicine Branch of the Chinese Medical Association and Deputy Leader of the Ninth Abdominal Group; Director of the Chinese Society of Ultrasound in Medicine Engineering, Deputy Chairman of the Abdominal Committee, and Deputy Chairman of the Committee on Superficial Organs and Peripheral Vessels; Vice Chairman of the Ultrasound Branch of the Guangdong Medical Association and Guangdong Medical Doctor Association; Chairman of the Ultrasound Branch of the Shenzhen Medical Association. Published more than 100 papers in national journals, over 90 papers in SCI-indexed journals, with the highest impact factor of **22.3**, and edited 5 professional books. Ranked in the top 10 national ultrasound medical scholars in 2022. Main research interests include abdominal and superficial organ ultrasound.

Fajin Dong, MD, Chief Physician of the Ultrasound Department at Shenzhen People's Hospital, Supervisor of Master's Students. Specializes in abdominal, superficial, and musculoskeletal ultrasound diagnosis and intervention therapy. Published over 60 SCI papers as the first/corresponding author (representative papers published in internationally renowned journals such as Medical Image Analysis, Research, and Nature Communications), led and participated in numerous national, provincial, and municipal projects. Serves as a committee member of the Ultrasound Branch of the Chinese Medical Association's Superficial and Vascular Group; Member of the Musculoskeletal Ultrasound Special Committee of the Chinese Medical Doctor Association & Standing Committee Member of the Interventional Physicians Branch Pain Treatment Group; Member of the Musculoskeletal Special Committee of the Chinese Society of Ultrasound in Medicine Engineering, among others.

Zhibin Huang, MD, is a resident of Ultrasound in The Second Clinical Medical College, Jinan University, China. He focuses on the clinical application of photoacoustic imaging and multi-modality imaging, especially the clinical diagnosis of diseases in breast and rheumatoid arthritics.

Sijie Mo, MD, is a resident of Ultrasound in The Second Clinical Medical College, Jinan University, China. Her fields of scientific interests: clinical application of photoacoustic imaging and multi-modality imaging, especially the clinical diagnosis of diseases in breast lesion.